UC Davis
UC Davis Previously Published Works

Title

Damage sensor role of UV-DDB during base excision repair

Authors

Jang, Sunbok
Kumar, Namrata
Beckwitt, Emily C
et al.

Peer reviewed

Damage sensor role of UV-DDB during base excision repair

Sunbok Jang[1,2], **Namrata Kumar**[2,3], **Emily C. Beckwitt**[2,5], **Muwen Kong**[2,5,*], **Elise Fouquerel**[2,6,**], **Vesna Rapi -Otrin**[4], **Rajendra Prasad**[7], **Simon C. Watkins**[8], **Cindy Khuu**[9,10], **Chandrima Majumdar**[9], **Sheila S. David**[9,10], **Samuel H. Wilson**[7], **Marcel P. Bruchez**[11,12,13], **Patricia L. Opresko**[2,6], **Bennett Van Houten**[1,2,3,5,#]

[1]Department of Pharmacology and Chemical Biology, School of Medicine, University of Pittsburgh, Pittsburgh, PA 15213, USA

[2]UPMC Hillman Cancer Center, University of Pittsburgh, PA 15213, USA

[3]Molecular Genetics and Developmental Biology Graduate Program, School of Medicine, University of Pittsburgh, Pittsburgh, PA 15261, USA

[4]Department of Microbiology and Molecular Genetics, School of Medicine, University of Pittsburgh, Pittsburgh, PA 15213 USA

[5]Molecular Biophysics and Structural Biology Graduate Program, Carnegie Mellon University and University of Pittsburgh, Pittsburgh, PA 15261, USA

[6]Environmental and Occupational Health, School of Public Health, University of Pittsburgh, Pittsburgh, PA 15213, USA

[7]Genomic Integrity & Structural Biology Laboratory, National Institute of Environmental Health Sciences, NIH, Research Triangle Park, NC 27709, USA

[8]Center for Biologic Imaging, University of Pittsburgh, Pittsburgh, PA 15261, USA

[9]Department of Chemistry, University of California, Davis, Davis, CA 95616, USA

[10]Biochemistry, Molecular, Cellular and Developmental Graduate Group, University of California, Davis, Davis, CA 95616, USA

[11]Molecular Biosensor and Imaging Center, Carnegie Mellon University, Pittsburgh, PA 15213, USA

[12]Department of Biological Sciences, Carnegie Mellon University, Pittsburgh, PA 15213, USA

#To whom correspondence should be addressed at: Bennett Van Houten, 5117 Centre Ave, Hillman Cancer Center, Research Pavilion, Suite 2.6, Pittsburgh, PA 15213, United States., Tel:+1 412 623 7762; Fax: +1 412 623 7761; vanhoutenb@upmc.edu.

*Present address: Department of Biochemistry and Molecular Biophysics, Columbia University, New York, NY 10032, USA
**Present address: Department of Biochemistry and Molecular Biology, Thomas Jefferson University and Sydney Kimmel Medical College, Philadelphia, PA 19107, USA

[13]Department of Chemistry, Carnegie Mellon University, Pittsburgh, PA 15213, USA

Abstract

UV-DDB, a key protein in human global nucleotide excision repair (NER), binds avidly to abasic sites and 8-oxo-guanine (8-oxoG), suggesting a non-canonical role in base excision repair (BER). We investigated whether UV-DDB can stimulate BER for these two common forms of DNA damage, 8-oxoG and abasic sites, which are repaired by 8-oxoguanine glycosylase (OGG1) and apurinic/apyrimidinic endonuclease (APE1), respectively. UV-DDB increased both OGG1 and APE1 strand cleavage and stimulated subsequent DNA polymerase β gap-filling activity by 30-fold. Single molecule real-time imaging revealed that UV-DDB forms transient complexes with OGG1 or APE1, facilitating their dissociation from DNA. Furthermore, UV-DDB moved to sites of 8-oxoG repair in cells and UV-DDB depletion sensitized cells to oxidative DNA damage. We propose that UV-DDB is a general sensor of DNA damage in both NER and BER pathways, facilitating damage recognition in the context of chromatin.

Keywords

INTRODUCTION

In mammalian cells, repair of the common oxidative lesion 8-oxo-guanine (8-oxoG) is mediated through base excision repair (BER), which is initiated by 8-oxoguanine-DNA glycosylase (OGG1, 39 kDa)[1]. OGG1 breaks the glycosidic bond between the base and sugar generating an abasic site, which is further processed by an associated apurinic/apyrimidinic (AP) lyase activity to generate a 3' phospho α,β-unsaturated aldehyde (3' dRP) moiety. AP endonuclease 1 (APE1, 35 kDa) can process this intermediate to generate a 3'OH and one base gap. OGG1 has a poor turnover rate that can be stimulated by human APE1 [2].

One important rate-limiting step during BER is access to DNA adducts in tightly packed chromatin in the nucleus. Several studies have shown that DNA lesions and repair intermediates wrapped around a nucleosome are poor substrates for glycosylases and APE1[3-6]. Furthermore, the orientation of a DNA lesion in a nucleosome also impacts the accessibility of glycosylase to initiate its repair[7-9]. Chromatin remodeling proteins and histone chaperones have been suggested to help overcome this barrier[10-12], but the nature of this processes remains unresolved[13-16].

A similar process of chromatin remodeling must occur during global genomic nucleotide excision repair (NER) of UV-induced photoproducts[17,18]. To this end, UV-damaged DNA-binding (UV-DDB) protein complex has been shown to play a major role in global genomic NER as the initial sensor of the two major types of UV-induced DNA lesions, the cyclobutane pyrimidine dimer (CPD) and (6–4) photoproduct (6–4PP)[19]. UV-DDB is a heterodimeric complex consisting of DDB1 (127 kDa) and DDB2 (48 kDa) that binds avidly

to UV-irradiated DNA[20]. In the nucleus UV-DDB, as part of CUL4A-RBX E3 ubiquitin ligase, acts to modify core histones around the sites of UV-lesions[21,22]. Mutations in the gene encoding DDB2 can give rise to the autosomal recessive disorder termed xeroderma pigmentosum complementation group E (XP-E) and skin cancer[23-26]. The absence of functional DDB2 in cells results in significantly delayed removal of 6–4PPs and overall reduced rate of CPD repair[27]. Interestingly, a survey of binding affinities for different DNA lesions revealed that UV-DDB binds more readily to abasic sites than CPDs[28]. Since abasic sites represent key intermediates in BER, we sought to determine if UV-DDB binding to 8-oxoG and abasic sites alters downstream processes in BER.

We found that UV-DDB stimulates OGG1 activity on 8-oxoG:C-containing substrates ~3-fold and APE1 cleavage of abasic sites up to 9-fold. Single molecule studies revealed that UV-DDB can form complexes on DNA with either OGG1 or APE1 and facilitates their dissociation. Finally, cellular experiments demonstrated that UV-DDB is rapidly recruited to sites of 8-oxoG formation and loss of UV-DDB activity sensitizes cells to an oxidant that primarily induces 8-oxoG lesions. Our current study provides novel insights into a new damage sensor role for UV-DDB in BER.

RESULTS

UV-DDB shows high affinity for base excision repair intermediates

UV-DDB has been shown to stimulate the removal of CPD five to six-fold in an in vitro system consisting of purified NER proteins[29]. However, despite this stimulation, the damage specificity of UV-DDB for CPD has been contested[28,30]. One study indicated that UV-DDB has little specificity for a DNA duplex containing a CPD[30], whereas a later study indicated increased specificity for CPD[28]. Interestingly, this study also indicated that UV-DDB has the highest affinity for an abasic site, followed by a CPD, and the lowest affinity was for unmodified DNA[28]. In fact, two separate groups have crystallized full length human[31] and zebrafish UV-DDB (lacking the N-terminus of DDB2)[32] complexed to a DNA fragment containing an abasic site. We therefore first sought to quantify UV-DDB binding affinities for undamaged DNA and four different types of DNA damage: CPD, tetrahydrofuran (THF, a stable abasic site analog), 8-oxoG:C and 8-oxoG:A. We performed electrophoretic mobility shift assays (EMSA; Fig. 1a and Supplementary Fig. 1b-f) and apparent equilibrium dissociation constants (K_d) were determined from the binding isotherms presented in Fig. 1a. Consistent with the report by Wood and colleagues[28], our data clearly demonstrate that UV-DDB binds to DNA containing a THF moiety with ~290-fold higher affinity (THF37; $K_d = 3.9 \pm 0.5$ nM) than non-damaged DNA (UD37; $K_d = 1108 \pm 95.5$ nM) and with 8-fold higher affinity than CPD (CPD37; $K_d = 30.4 \pm 2.4$ nM). Surprisingly, UV-DDB also had a ~7-fold increase in specificity for a 37 bp duplex containing either an 8-oxoG:C pair (8-oxoG37(G:C); $K_d = 159.6 \pm 12.4$ nM), or 8-oxoG:A pair (8-oxoG37(G:A); $K_d = 163.8 \pm 14.8$ nM) as compared to non-damaged DNA, see Table 1.

UV-DDB stimulates OGG1 excision and subsequent AP lyase activity

Having confirmed that 8-oxoG lesions and abasic sites, key substrates in the BER pathway, are bound tightly by UV-DDB, we asked whether UV-DDB binding can alter human OGG1

incision kinetics (Fig. 1b). OGG1 is the primary enzyme responsible for removal of 8-oxoG during BER. The glycosylase activity of OGG1 releases the oxidized guanine from the sugar moiety; yet the subsequent AP lyase activity of OGG1 is much weaker than its glycosylase activity, causing the protein to be product inhibited and stay bound to an abasic site[2]. Incubation of a 37 bp substrate containing an 8-oxoG:C [50nM, 8-oxoG37(G:C)] with increasing amounts of OGG1 (0–250 nM) alone led to accumulation of incised products (Supplementary Fig. 2b). Time course studies with two different preparations of OGG1 displayed slow incision kinetics and are consistent with previous published work[2] (Fig. 1c lanes 1–8 and Fig. 1d open circles). Additional EMSA experiments showed that OGG1 binds THF37 with ~3-fold higher affinity than 8-oxoG37(G:C) (Supplementary Fig. 3a). These data agree with the concept that OGG1 binds more readily to abasic sites, and thus product release is rate limiting for OGG1, as reported previously[2]. We hypothesized that UV-DDB may facilitate OGG1 AP lyase activity and product release, in a manner similar to APE1-mediated turnover of OGG1[2]. Time course experiments in the absence and presence of an optimal concentration of UV-DDB (16 nM) (as determined in Supplementary Fig. 2d,e) indicated that UV-DDB can enhance OGG1 mediated incision of DNA ~3-fold (Fig. 1c,d). Since the kinetics of OGG1 incision is relatively slow, we verified that OGG1 remains active and that UV-DDB can stimulate OGG1 after two hours of pre-incubation without UV-DDB (Supplementary Fig. 2f,g). Furthermore UV-DDB was able provide stimulation of OGG1 beyond that observed with APE1, which is known to stimulate the turnover of OGG1[2] (Supplementary Fig. 2h,i). Since UV-DDB binds specifically to 8-oxoG:A pairs we tested whether MUTYH, a monofunctional glycosylase which removes the A across from an 8-oxoG adduct, is also stimulated by UV-DDB. As shown in Supplementary Fig. 2j,k, UV-DDB, over a 100-fold concentration range (0.5–50 nM), stimulated the glycosylase activity of MUTYH (10 nM) ~4–7-fold. EMSA experiments with OGG1 and UV-DDB show that UV-DDB, which has a 9-fold higher affinity for abasic sites than OGG1, can displace OGG1 from abasic sites (Supplementary Fig. 3c,d). Taken together, these data suggest that UV-DDB facilitates the enzymatic turnover of OGG1 and MUTYH by prompting displacement of these enzymes from their products.

UV-DDB stimulates APE1 incision activity

Since UV-DDB binds to abasic sites (Fig. 1a) with similar affinity as APE1 (Supplementary Fig. 3b), we next assessed whether UV-DDB influences APE1 incision of these substrates (Fig. 1e). The addition of 10 nM UV-DDB to 0.5 nM APE1 caused a maximum stimulation effect (around 8-fold increase) (Fig. 1f,g). Initial rate experiments indicate that UV-DDB is enhancing the rate at which APE1 binds and incises abasic sites (Supplementary Fig. 2n,o). We also discovered that stimulation of APE1 incision activity by UV-DDB was concentration dependent reaching a maximum (10 nM) at around 2.5-fold over the K_d (3.9nM) and then subsequent decline at higher concentrations (Supplementary Fig. 2l,m). These results suggest that very stable dimerization of UV-DDB at a damaged site, which occurs at higher protein concentrations (see EMSA in Supplementary Fig. 3c)[33], may block APE1 access to abasic sites, eliminating any enhanced activity. These incision kinetic data, when combined with the affinity data, indicate that UV-DDB may stimulate the turnover of APE1 activity or facilitate product release during the APE1 catalytic cycle during base excision repair. This concept was tested in more detail below.

UV-DDB facilitates dissociation of OGG1 or APE1 from abasic DNA

We next sought to understand the mechanism of UV-DDB stimulation of OGG1/APE1 incision activity and tested the hypothesis that equal molar or excess (10-fold) UV-DDB would increase the rates of dissociation of OGG1 or APE1 from abasic sites, thus increasing their rates of turnover. We used a single molecule approach involving a DNA tightrope assay to follow the rates of OGG1 or APE1 dissociation. In this experiment, OGG1 and APE1 were labeled with 605 nm quantum dots (Qdots) using an antibody sandwich approach in which a primary mouse-anti-His antibody was bound to a His-tagged OGG1 or APE1 protein, followed with goat-anti-mouse secondary antibody-coated 605 Qdots (Fig. 2a). Qdot-labeled OGG1 or APE1 was observed in the absence or presence of unlabeled UV-DDB on DNA tightropes containing one abasic (THF) site every 2 kb (see Methods for details) for a total of 5 minutes, and the number of Qdot-labeled proteins dissociating during that time was noted. The addition of unlabeled UV-DDB to either OGG1 or APE1 did not substantially change the linear diffusion of these proteins along DNA (Fig. 2b,c). However, both proteins displayed a 2 to 3-fold increase in the frequency of dissociation (during a 5 minute observation window) when UV-DDB was added (Fig. 2d,e). Addition of equal molar or 10-fold excess of UV-DDB to OGG1 decreased OGG1's half-life from 863 seconds to 353 or 182 seconds, respectively (Fig. 2f). Addition of equal molar or 10-fold excess of UV-DDB also decreased the half-life of APE1 on THF DNA from 942 seconds to 335 or 270 seconds, respectively (Fig. 2g). These data suggest that UV-DDB facilitates the dissociation of OGG1 and APE1 molecules on THF-containing DNA, which may contribute to the stimulation of the incision kinetics observed in Fig. 1. These data further support the idea that UV-DDB can displace OGG1 from abasic sites, as was observed in EMSA experiments (Supplementary Fig. 3c,d).

UV-DDB can co-localize with OGG1 or APE1 on DNA containing abasic sites

Since both UV-DDB and OGG1/APE1 are capable of binding to abasic sites individually, we sought to further investigate the potential interaction of UV-DDB with these two BER proteins on DNA containing abasic sites. We developed an orthogonal labeling strategy for direct dual-color fluorescence imaging of Flag-tagged UV-DDB, labeled with a biotinylated goat-anti-Flag primary antibody and streptavidin-coated 705nm Qdot, with His-tagged OGG1 or APE1, labeled with 605nm Qdots as described above (Fig. 3a). Qdot-labeled UV-DDB was first injected into a flow cell containing DNA tightropes with one abasic site (THF) every 2kb followed by injection of Qdot-labeled OGG1 or APE1. After injection all flow was stopped. Due to the transient nature (mobility and dissociation) of UV-DDB, APE1, and OGG1 binding to damaged DNA, we reasoned that co-localization might be a relatively rare event. We found that co-localization of OGG1/UV-DDB or APE1/UV-DDB accounted for 9.5% or 9.4% of all particles, respectively (Fig. 3b,e). Some of these co-localized molecules (examples in Fig. 3c,f) were found to diffuse on the DNA together, suggesting direct interactions on DNA, however the overall motion of the repair proteins did not change substantially when complexed together (Supplementary Fig. 4a-f). The kymographs of merged channels (Fig. 3d,g) show co-localization (yellow) of green and red signals, indicating specific binding of OGG1 or APE1 with UV-DDB (see additional kymographs in Supplementary Fig. 4g,h and Videos S1 and S2). Also note that UV-DDB

helps to dissociate OGG1 (Video S1, Fig. 3d). Taken together, these data suggest that UV-DDB can associate and migrate together with OGG1 or APE1 on DNA.

Involvement of UV-DDB in base excision repair of oxidative damage in living cells.

Having shown that UV-DDB greatly stimulates APE1 incision, we next sought to determine whether UV-DDB stimulates an in vitro human BER reaction. In this experiment, DNA duplex containing an abasic site across from a G is cleaved by APE1 and DNA Polymerase β (Pol β) incorporation of $[\alpha-^{32}P]$-dCTP is monitored over time in the presence or absence of UV-DDB (Fig. 4a). Pol β incorporation of $[\alpha-^{32}P]$-dCTP in a one nucleotide gap was stimulated ~30-fold by UV-DDB (Fig. 4b, lanes 1 and 9). The formation of full-length, ligated product (lanes 2–5) in the presence of DNA Ligase III indicate that UV-DDB does not inhibit subsequent steps in BER. These data suggest that while UV-DDB has affinity for a nicked site, it does not interfere with Pol β incorporation or DNA Ligase III activity during the BER reaction.

To confirm that UV-DDB stimulates BER in living cells, we performed a series of cell survival experiments. Potassium bromate is a strong oxidant that induces 8-oxoG lesions in DNA[34]. Previous studies have shown that other NER factors, such as XPC, play an important role in 8-oxoG recognition and removal[34,35]. In order to test whether UV-DDB plays an important role in protecting cells against oxidative DNA damage, cells were treated with potassium bromate and cell growth was determined. Two lymphoblastoid cell lines from patients with XP-E phenotype showed increased sensitivity in a short-term (72 hour) growth assay, as compared to two control cell lines from two individuals with apparently normal NER (Supplementary Fig. 5b). However, these differences did not reach statistical significance and we therefore performed a DDB2 knockdown experiment. siRNA depletion of UV-DDB in an immortalized fibroblast line (BJ-hTERT) (Supplementary Fig. 5c) showed significant sensitivity to potassium bromate (Fig. 4c) in a long-term (7 day) growth assay. Knocking down DDB2 did not decrease the expression levels of OGG1 or APE1, confirming that the sensitivity was solely due to the effect of DDB2 (Supplementary Fig. 5c).

We next sought to determine whether UV-DDB is recruited directly to sites of 8-oxoG damage. We targeted 8-oxoG to the telomeric regions of DNA in vivo using a novel chemoptogenetic approach[36]. This innovative technology consists of a fluorogen activating peptide (FAP) fused to the telomere shelterin protein, telomeric repeat-binding factor 1 (TRF1), which binds specifically to telomeric sequences. The FAP binds a photosensitizer (MG2I) with picomolar affinity, which when excited by 660 nm light produces singlet oxygen and subsequent 8-oxoG damage only at telomeric sequences[37] (Fig. 4d). U2OS cells expressing the TRF1-FAP construct containing mCherry-DDB2 were treated with the MG2I dye (100 nM) and 660 nm light for 10 minutes and immediately harvested for immunofluorescence. UV-DDB can be found co-localized with fluorescent PNA-FISH probes at telomeres immediately after dye plus light treatment (~10 min), but not in control cells (Fig. 4e). The difference between percent co-localization of UV-DDB at telomeres in control cells (1.3 ± 0.16 %) versus that in cells treated with dye plus light (19.6 ± 2.24 %) was highly significant ($p < 0.001$) (Fig. 4f). A time course experiment showed that the DDB2 foci significantly decreased in the first 30 minutes after damage and returned to

control levels by two hours, indicating that the telomeres are being repaired (Fig. 4g and Supplementary Fig. 5d). Interestingly, we found that OGG1 co-localized with DDB2 at the telomeres and the OGG1 foci disappeared with slower kinetics than that of DDB2. It is worth noting that the maximum recruitment of OGG1 to damaged telomeres occurs at 30 minutes after dye plus light, which is later than DDB2, suggesting an early role of UV-DDB in allowing OGG1 to access the damage site. We also observed a slight increase in the number of DDB2 foci at one hour (as compared to 30 minutes) after damage induction. It is possible that UV-DDB is playing two roles in BER at 8-oxoG damaged sites, first perhaps by opening chromatin and second in working with APE1 to help OGG1 turnover to further recruit downstream proteins (Fig. 4g **and** Supplementary Fig. 5d).Furthermore, live-cell imaging showed that mCherry-DDB2 was recruited to telomeres immediately after the damage was induced (Video S3). Together these data provide strong support for a direct role of UV-DDB in the processing of 8-oxoG adducts in human cells.

DISCUSSION

Here, we report a novel function for UV-DDB in base excision repair of 8-oxoG. We found that UV-DDB, through its robust recognition of abasic sites[28,38], provides a remarkable stimulation of OGG1 glycosylase/lyase and MUTYH glycosylase activities, as well as APE1 incision activity. In reconstituted BER reactions with purified proteins and a substrate containing an abasic site, UV-DDB was able to stimulate Pol β gap-filling by over 30-fold. Single molecule studies demonstrated that this phenomenon is mediated by the ability of UV-DDB to facilitate the dissociation of OGG1 and APE1. Cell experiments demonstrated that lower UV-DDB expression sensitized cells to an oxidant known to induce 8-oxoG lesions. Future studies will focus on constructing DDB2 knockout cell lines to determine the precise role of UV-DDB in protecting cells from oxidant injury. Finally, using a highly innovative chemoptogenetic approach[36,37], we demonstrated that UV-DDB is rapidly recruited to 8-oxoG lesions undergoing repair. Together these data implicate UV-DDB as being a general damage sensor during the removal of 8-oxoG by BER.

BER proteins have been suggested to work in a highly concerted manner through substrate channeling[39]. For example, APE1 has been reported to stimulate the slow turnover rate of OGG1[2]. OGG1 has also been reported to cooperate with APE1 or NEIL1 to facilitate enzymatic turnover [40,41]. Furthermore, APE1 has been found to be stimulated by PARP1[42] or the Rad9-Rad1-Hus1 (9–1-1) complex[43], and OGG1 has been suggested to be stimulated by RAD52[44], indicating that cross-talk between multiple DNA repair pathways is possible. To this end, we found that the canonical NER protein UV-DDB stimulates the AP lyase activity of OGG1 by increasing the rate of OGG1 turnover, in a protein concentration-dependent manner. Protein facilitated dissociation has been observed previously by Marko and coworkers[45,46]. They propose that a protein bound to DNA undergoes domain specific transient micro-dissociations from the DNA, whereas macro-dissociation occurs when multiple domains dissociate simultaneously or if another protein molecule binds to the segment of DNA that has been vacated by the domain micro-dissociation. We believe that the action of UV-DDB to avidly bind to abasic sites helps facilitate the turnover of OGG1, MUTYH, and APE1. APE1, whose incision activity was greatly stimulated by UV-DDB, showed less pronounced dissociation effects by UV-DDB. These data indicate that either

there is some upper limit to UV-DDB's facilitated dissociation rate and/or that UV-DDB can increase the catalytic efficiency of APE1. APE1 displays rapid rates of diffusion along DNA, and even though its k_{cat} is in the range of 100/sec[47], its rapid diffusion along DNA at approximately 1 bp/4–5 μsec[48], may allow it to occasionally skip over an abasic site, and thus is somewhat "blinded" due to its rapid searching rate. Since UV-DDB and APE1 were observed to bind on DNA together, UV-DDB may cause APE1 to pause at a site of damage so to increase the likelihood of "seeing" the abasic site, facilitating catalysis and incision of the sugar phosphate backbone.

Given that our biochemical and biophysical studies strongly suggest direct involvement of UV-DDB in BER, we further verified this concept using cell experiments. Potassium bromate is a strong oxidant that induces significant levels of 8-oxoG[34]. We showed depletion of DDB2 with siRNA in telomerase immortalized human fibroblasts also increased sensitivity to potassium bromate. Finally, using a novel chemoptogenetic approach to introduce singlet oxygen-induced 8-oxoG damage at telomeres[36,37], we demonstrated that UV-DDB was rapidly recruited to damaged regions and participates in their repair. Together, these data suggest that UV-DDB helps process 8-oxoG damage in human cells. Along with previous work that suggested that both XPA[35] and XPC[34] work with BER enzymes to help stimulate the removal of 8-oxoG, our data indicate an important cross-talk between NER proteins and BER repair proteins. In this regard, it is interesting to note that Sancar and co-workers, using a reconstituted human NER system, showed that 8-oxoG was apparently recognized and removed as part of the oligonucleotide, consistent with the idea that NER can act on oxidative lesions[49]. Finally, these data suggest that UV-DDB's damage repertoire includes other DNA modifications beyond UV-induced photoproducts. In support of this idea, Seidman and coworkers showed that UV-DDB is rapidly recruited to sites of angelicin-thymine monoadducts[50].

In conclusion, our results demonstrate that the UV-DDB plays a damage sensor role during BER by interacting with and stimulating OGG1 and APE1 activities. We believe that UV-DDB is critically involved in maintaining genomic stability by facilitating these early steps of BER. Based on our current studies, we propose a new working model for processing 8-oxoG by BER (Fig. 5). There are three functional steps that compose the repair of oxidative damage in DNA: lesion recognition / strand scission, DNA gap tailoring, and DNA synthesis / ligation. Our data are consistent with rapid recruitment of UV-DDB to 8-oxoG damaged sites within chromatin. UV-DDB as part of Cul4A-RBX complex (not shown), may help to identify 8-oxoG in the context of a nucleosome allowing access by BER proteins. It has been shown that OGG1 and APE1 have difficulty processing lesions in DNA wrapped around a nucleosome[7,12,16] and it is not clear how base damage is efficiently recognized in the context of chromatin[4,11,13]. Furthermore, OGG1 remains tightly bound to the abasic DNA upon removal of the flipped out 8-oxoG base and has a very slow rate of strand scission. This OGG1/AP DNA post-glycosylase complex is recognized by APE1 or UV-DDB, inducing OGG1 turnover. We believe that due to its high affinity for abasic sites, UV-DDB may help the turnover of other glycosylases. The stimulation of MUTYH removal of an A across from 8-oxoG supports this hypothesis. UV-DDB is also recruited to the remaining nicked abasic site to stimulate APE1-induced incision. This newly formed single-base gap is recognized by DNA Pol β and UV-DDB stimulates incorporation of dNTP into

the gap. It is also expected that PARP1 and the XRCC1/LIGIII heterodimer work together for the completion of repair (not shown). The experiments presented here suggest a new level of coordination in the BER pathway orchestrated by UV-DDB with OGG1, MUTYH, and APE1 in the initial recognition and processing steps. It is interesting to note that loss of even one allele of DDB2 causes increased spontaneous tumors in mice[51-53]. Future studies will explore the role of UV-DDB in damage recognition of BER intermediates wrapped around nucleosomes and the role played by its associated E3 ligase (CUL4A/RBX) during BER.

METHODS

Expression and purification of recombinant UV-DDB, OGG1, MUTYH, and APE1

Recombinant full-length UV-DDB (DDB1-DDB2 heterodimer) was expressed in Sf9 cells, co-infected with recombinant baculovirus of DDB1-His$_6$ and DDB2-Flag as performed previously [31]. Briefly, DDB1-His$_6$ and DDB2-Flag were purified using 5ml His-Trap™ HP column pre-charged with Ni^{2+} (GE Healthcare) and anti-FLAG M2 affinity gel (Sigma). The pooled anti-FLAG eluates were size fractionated on a HiLoad 16/60 Superdex 200 column (Amersham Pharmacia) in UV-DDB storage buffer (50mM HEPES, pH 7.5, 200mM KCl, 1mM EDTA, 0.5mM PMSF, 2mM DTT, 10% glycerol and 0.02% sodium azide). Purified fractions of DDB1-DDB2 complex from the Superdex200 were aliquoted and flash frozen with liquid nitrogen and stored at −80°C. Recombinant human OGG1 protein was purchased from Novus Biologicals or purified from bacterial cells as a GST fusion as previously described [54]. Mouse MUTYH was purified as described previously[55]. Recombinant WT or a catalytically-dead triple mutant (K87E/E96Q/D210N) His-tagged human APE1 was expressed in *E. coli* and purified as previously described [47,56]. DNA Pol β was purified as previously described [57]. Uracil glycosylase was purified as previously described [58]. DNA ligase III was purified as previously described [59]. Purified APE1, OGG1, and UV-DDB proteins are shown in Supplementary Fig. 1a.

Preparation of EMSA DNA substrate with fluorescein labels at either the 5' or 3' end.

The 37bp duplex DNA substrates used for EMSA experiments were prepared by annealing single stranded oligos at 95°C for 5 minutes and then cooled to room temperature for 1 hour by turning off the heating device. The AP37 duplex DNA was prepared through reaction with Uracil DNA glycosylase (NEB, USA).

The following oligonucleotides were used:

<u>UD37</u>: 5'CCG AGT CAT TCC TGC AGC GAG TCC ATG GGA GTC AAA T 3' and 6FAM-5'- ATT TGA CTC CCA TGG ACT CGC TGC AGG AAT GAC TCG G-3' (IDT, USA)

<u>THF37</u>: 5'CCG AGT CAT TCC TGC AGC G**X**G TCC ATG GGA GTC AAA T-3'-6FAM and 5'-ATT TGA CTC CCA TGG ACT CGC TGC AGG AAT GAC TCG G-3', where **X** represents Tetrahydrofuran (IDT, USA)

<u>CPD37</u>: 5'-CCG AGT CAT TCC TGC AGC GA**Y** CCA TGG GAG TCA AAT-3' (Y=CPD) and 6FAM-5'-ATT TGA CTC CCA TGG AAT CGC TGC AGG AAT GAC TCG G-3', where **Y** represents a cyclobutane pyrimidine dimer (Trilink, USA)

<u>8-oxoG37(G:C)</u>: 5'-CCG AGT CAT TCC TGC AGC GA**Z** TCC ATG GGA GTC AAA-3'-FldT and 5'-ATT TGA CTC CCA TGG ACT CGC TGC AGG AAT GAC TCG G-3', where **Z** represents 8-oxoG (Midland Certified Reagent Co, USA)

<u>8-oxoG37(G:A)</u>: 5'-CCG AGT CAT TCC TGC AGC GA**Z** TCC ATG GGA GTC AAA T-3' and 5'-A TTT GAC TCC CAT GGA ATC GCT GCA GGA ATG ACT CGG-3'-6FAM, where **Z** represents 8-oxoG (Trilink, USA)

Equilibrium dissociation constant determination from electrophoretic mobility shift assay (EMSA)

To determine the equilibrium dissociation constants of UV-DDB binding to various DNA lesions we conducted electrophoretic mobility shift assays with fluorescein-modified DNA substrates. DNA substrates, held constant at 8nM, were mixed with increasing amounts of UV-DDB and incubated for 20 minutes at room temperature in reaction buffer (20mM HEPES, pH 7.5, 150mM NaCl, 5mM $MgCl_2$, 2mM DTT, 5% glycerol, 0.5mg/ml BSA). A 5 µl aliquot of each reaction was loaded on a 5% polyacrylamide (37.5:1, acrylamide:bis) native gel, in duplicate, and run at 100V for 50 minutes at 4°C in 1/2X TBE with 5 mM $MgCl_2$. Gels were imaged using a laser scanner for fluorescence (Typhoon, Amersham). The percentage of total DNA bound by protein was determined by measuring the band intensity present in the bound states and dividing by the total band intensity in the lane. Background signals from blank regions of the gel were subtracted from the signal intensities obtained from bands. The percentage of DNA bound in each reaction was plotted against the concentration of UV-DDB and the binding isotherm was fit to the following equation using nonlinear regression in GraphPad Prism:

$$\% \, DNA \, Bound = 100 \times \frac{(D + P + K_d) - \sqrt{(D + P + K_d)^2 - 4DP}}{2D}$$

where K_d is the equilibrium dissociation constant, P is the total protein concentration, and D is the total DNA concentration, all in units M, as adapted from ref. [60]. Unlike other common models for fitting binding data that assume DNA concentration is well below the K_d, this quadratic equation takes into account the DNA concentration. When the DNA concentration in a binding reaction is within the range of the K_d, a significant fraction of the protein will be bound to the DNA, and thus total protein concentration cannot be used to approximate the amount of free protein, as discussed briefly in ref. [61].

Enzyme cleavage assays

OGG1 and MUTYH activity assays.—Reactions were carried out in a volume of 10 µl containing OGG1 incision buffer (20mM HEPES, pH 7.9, 50mM NaCl, 1mM $MgCl_2$, 1mM DTT), 50nM of fluorescein-labeled 8-oxoG-containing duplex DNA (8-oxoG37(G:C) or 8-oxoG37(G:A), described above) and the indicated amount of OGG1 or MUTYH and UV-

DDB. Reactions were incubated at 37°C for each time point (up to 4hrs) and rapidly quenched by adding an equal volume of gel loading buffer (2X formamide-dye solution), heated at 95°C for 5mins then cooled on ice for 5mins. For MUTYH experiments, 0.1M NaOH was included in the quenching step to induce DNA nicking at the abasic site. The reaction product was separated by electrophoresis on 10% denaturing polyacrylamide gel and visualized by using a laser scanner for fluorescence (Typhoon, Amersham). The substrate and product bands were quantified using GelAnalyzer software.

APE1 incision assay.—APE1 incision reactions were carried out in a reaction mixture (10 μl) containing APE1 incision buffer (20mM HEPES, pH 7.5, 150mM NaCl, 1mM DTT, 5% glycerol, 10mM $MgCl_2$), 50nM of fluorescein-labeled dsDNA containing THF (THF37, described above), and the indicated amount of APE1 and UV-DDB. For the initial rate experiments, the 34 bp DNA substrate was 200 nM. Reactions were incubated at room temperature for each time point (up to 70mins) and stopped by adding an equal volume of 2X formamide-dye solution. Samples were incubated at 95°C for 10mins and then quickly chilled on ice for 10mins. The reaction product was separated by 10% denaturing polyacrylamide gel and visualized by using a laser scanner for fluorescence (Typhoon, Amersham). The substrate and product bands were quantified using GelAnalyzer software.

Reconstituted human BER assay

The BER assay was performed in a final reaction mixture volume of 20 μl, as described previously [62]. Briefly, the repair reaction mixture, assembled at 0–4 °C, contained 50 mM HEPES, pH 7.5, 20 mM KCl, 5 mM $MgCl_2$, 0.5 mM EDTA, 2 mM DTT, 2 mM ATP, 5 μM [α–^{32}P]-dCTP (specific activity, 1×10^6 dpm/pmol), a 34-base pair uracil-containing DNA (200 nM) pretreated with UDG, DNA polymerase β (Pol β) (20 nM), with or without DNA ligase III (250 nM), and/or UV-DDB (50 nM), as indicated. The repair reactions were then initiated by addition of 1 nM APE1 and transferring the reaction mixture to 37 °C. Aliquots (4.5 μl) were removed for analysis at the indicated times. The reaction was terminated by addition of an equal volume of DNA gel loading buffer (95% formamide, 20 mM EDTA, 0.02% bromophenol blue, and 0.02% xylene cyanol). After incubation at 75 °C for 2 min, the reaction products were separated by electrophoresis in a 16% polyacrylamide gel containing 8 M urea in 89 mM Tris-HCl, pH 8.8, 89 mM boric acid, and 2 mM EDTA. A Typhoon PhosphorImager was used for gel scanning and imaging, and the data were analyzed by ImageQuant software.

The following oligonucleotides were used in these assays:

BER-U: p5'- CTG CAG CTG ATG CGC UGT ACG GAT CCC CGG GTA ddC-3' (IDT, USA)

APE1-THF: 6FAM-5'-CTG CAG CTG ATG CGC **X**GT ACG GAT CCC CGG GTAC-3', where **X** represents THF (IDT, USA)

APE1-U: 6FAM-5'-CTG CAG CTG ATG CGC **U**GT ACG GAT CCC CGG GTAC-3', where **U** represents Uracil (IDT, USA)

Single Molecule DNA Tightrope Assay

Single molecule DNA tightrope assay was performed as described previously[33,48,63]. Briefly, poly-L-lysine (Wako Pure Chemicals) coated silica beads (5 μm; Polysciences Inc.) were deposited onto a PEG-treated coverslip (24 × 40 mm; Corning) in a custom flow cell. Defined-lesion (abasic site) substrates were strung up across the beads via hydrodynamic flow. DNA substrates were made by tandem ligation of pSCW01 plasmid (~2 kb) with a single, site specific THF modification and proximal biotinylated thymine. Prior to imaging, purified His-tagged OGG1 or APE1 were labeled with secondary antibody-coated 605nm quantum dots (Qdots; Invitrogen) through α-His primary antibody (Qiagen). For UV-DDB facilitated dissociation experiments, quantum dot-labeled OGG1 or APE1 were injected into the flow cell at final concentrations of 2.6nM with 1X or 10X UV-DDB conjugated to goat α-Flag primary antibody. For co-localization experiments, purified UV-DDB was conjugated to streptavidin-coated 705nm Qdots through biotinylated goat α-Flag primary antibody (Bethyl), and quantum dot-labeled OGG1, APE1, or UV-DDB were injected into the flow cell at final concentrations of 2.6nM, 2.6nM, or 3.1nM, respectively. We conjugated each protein in separate reaction tubes and injected into the flow cell separately for dual-color experiments; flow was stopped during the observation period. Furthermore, we performed a control experiment to check whether there is any unwanted interaction between 705Qdot-labeled UV-DDB (DDB1 is His-tagged) and α-His primary antibody conjugated to 605Qdots. We injected 705Qdot conjugated UV-DDB into the flow cell and then injected 605Qdot conjugated with α-His primary antibody, and observed for 4 hours. During this time, 20 particles were recorded, but none were co-localized. All binding experiments were carried out in tightrope buffer (25mM HEPES, pH 7.5, 150mM NaCl, 10mM $MgCl_2$, 0.1 mg/ml BSA (Roche), 50nM biotin, and 1mM DTT). Labeled proteins were visualized using oblique angle fluorescence (Nikon Eclipse Ti inverted microscope with Nikon 100X TIRF objective and 1.45 numerical aperture) with a 488 nm laser (power 1–2 mW) at the back focal plane to excite Qdots and the appropriate emission filter (Chroma) applied at RT. Images were acquired using Nikon Elements (4.2) and exported as TIFF stacks for kymograph processing and analysis in ImageJ (NIH). Differences between dissociation rates and motility fractions were assessed by one-way ANOVA.

Cell lines

The U2OS-TRF1-FAP stable line was obtained by transfecting pLVX-FAP-mCer-TRF1 plasmid in U2OS cells followed by selection in 500μg/ml G418 (Gibco) and single cell cloning for the selection of cells harboring exclusive expression of FAP-mCer-TRF1 construct at telomeres. Cells were cultured at 5% oxygen in Dulbecco's Modified Eagle Medium (DMEM) containing 4g/l glucose (Gibco) and supplemented with 10% Fetal Bovine Serum (Gibco), 1x penicillin/streptavidin (Life Technologies) and 500μg/ml G418[37]. These cells were transfected with an mCherry-DDB2 plasmid, (a mouse CDS with mCherry at the C-terminus, generously provided by Dr. Wim Vermeulen), sorted by flow cytometry, and cultured in 5% O_2 in DMEM (10% FBS, G418). OGG1-GFP (generously provided by Dr. Anna Campalans) was transiently transfected for the time-course experiments. BJ-hTERT cells were purchased from ATCC and cultured in DMEM (10% FBS). Normal (GM07524 and 705ori) and XPE (XP23PV and XP25PV) lymphoblastoid cell lines were as

reported[24] and cultured in RPMI-1640 (15% FBS). All cell lines tested negative for mycoplasma.

Cell Proliferation and Survival Assay

Normal and XPE lymphoblastoid cells were treated with $KBrO_3$ (0–20mM) for 1 hour at 37°C and then plated in 96-well plates at a density of 2000 cells/ well. 72 hours later, cell growth was estimated using the CyQUANT Direct Cell Proliferation Assay Kit (Molecular Probes; #C35011), according to manufacturer's directions. For the cell survival assay, BJ-hTERT cells were plated and transfected with either scrambled or DDB2 siRNA (Dharmacon)[64]. The next day, cells were trypsinized and plated in triplicate at equal densities in 60mm dishes. The following day, cells were treated with $KBrO_3$ (0–20mM) for 1 hour at 37°C. Fresh media was added and the cells were allowed to recover for 7 days. Cells were counted using a cell counter (Innovatis/ Bio-Rad) and a survival curve was plotted. Knockdown by siRNA was validated 72 hours after transfection by western blot for DDB2 (Rb-DDB2; Abcam #181136) (Supplementary Fig. 5b).

The following siRNAs were used in these assays:

Scrambled siRNA: UUC UCC GAA CGU GUC ACG U (Pharmacon, USA)

DDB2 siRNA1: CAA CUA GGC UGC AAG ACU U (Pharmacon, USA)

DDB2 siRNA2: GAU AUC AUG CUC UGG AAU U (Pharmacon, USA)

DDB2 recruitment at telomeres

U2OS-TRF1-FAP-(mCherry-DDB2) cells were plated on coverslips. OGG1-GFP was transiently transfected for the time-course experiments. The next day, cells were treated with dye (100nM MG2I; 15 minutes) and light (660 nm, 10 minutes), then fixed with 4% paraformaldehyde for 10 minutes. Cells were washed with PBS 3 times, and permeabilized with 0.2% Triton X-100, followed by blocking for 1 hour at room temperature (10% goat serum, 1% BSA in PBS). mCherry antibody (1:500; Abcam #ab167453) and GFP antibody (for the time-course experiment) (1:500, Santa Cruz #B-2) were added to the cells and incubated overnight at 4°C. The next day, cells were washed 3 times with PBS, and incubated with anti-rabbit secondary antibody (1:1000; Cell Signaling Cat# 8889S) for 1 hour at room temperature. After 3 PBS washes, cells were fixed again with 4% paraformaldehyde for 10 minutes, washed again in PBS, and dehydrated in 70%, 90% and 100% ethanol for 5 minutes each. 0.1 μM PNA probe (PNA Bio, F1004; (CCCTAA)$_3$-Alexa488) was diluted in hybridization solution (70% Di Formamide, 1X Maleic acid, 10mM Tris pH 7.5, 1X $MgCl_2$) and incubated at 95ºC for 3–5 minutes. After letting the coverslips dry for 2 minutes, cells were hybridized for 10 minutes at 95ºC and incubated at room temperature for 2 hours in a humid chamber box, protected from light. Next, cells were washed twice in hybridization wash buffer (70% formamide, 10mM Tris HCl pH 7.5) for 15 minutes each. After 3 washes in PBS, cells were incubated with DAPI (1:10,000) for 10 minutes at room temperature. Cells were rinsed once with PBS and dH_2O, before mounting on slides with Prolong Diamond Anti-Fade (Catalog #P36970; Molecular Probes).

Images were acquired on the Nikon Ti inverted fluorescence microscope, with a Z stack of 0.2μm, and deconvoluted and analyzed using NIS Elements advance research software. The region of interest (ROI) tool was used to label the nuclei. Using the measurement tab, a separate binary layer was created for the DDB2 foci and the telomere foci. Using the intersection tool, a third binary layer was created, that identified the co-localized foci. The intensity threshold for each channel was kept the same for all samples and the foci counts were exported to Excel for analysis.

Unpaired t-test or one-way ANOVA was used to compare the survival curves or the quantification of DDB2 foci recruited at the telomeres. All the analyses were performed on GraphPad Prism software.

Live-cell imaging was done using a Nikon (Tokyo, Japan) Ti-E inverted microscope equipped with a Bruker (Madison, WI) Opterra confocal scan head, an Oxxius (Paris, France) Laser Launch and Photometrics (Tucson, AZ) Prime 95B camera. Cells stably expressing mCherry-DDB2 and TRF1-FAP were cultured in 35mm Mattek dishes (Ashland, MA). The mid-plane of cells in a 90% confluent monolayer was selected and 20 individual imaging positions were chosen using the 561nm line the Opterra confocal with a 35mm slit and a 100× 1.49 Plan Apochromat TIRF objective to selectively excite the mCherry-DDB2. Once image positions were selected the Y scan axis on the scan head was transiently disabled and the central region (in XY and Z) was line scanned using the 640nm line at full power (85mW at the end of the fiber) for 8 seconds. The stimulation line was diffraction limited in size in covering the full X axis of the imaging field, 200nm in Y and 500–600nm in Z. Full field midplane images were then collected over time using the 561 nm line and imaging conditions that caused no fluorophore bleaching (100ms exposure, minimal laser power), images were collected every 20 seconds for 1 hour. Collected data sets were deconvolved using NIS elements and rendered using the same software.

Data Availability Statement.

Source data for Figure 1a,d,g and Figure 4c,f,g are available with the paper online. Further information and requests for resources and reagents should be directed to and will be fulfilled by corresponding author, Bennett Van Houten (vanhoutenb@upmc.edu)

Supplementary Material

Refer to Web version on PubMed Central for supplementary material.

Acknowledgements.

REFERENCES

1. Friedberg EC et al. DNA repair: from molecular mechanism to human disease. DNA Repair (Amst) 5, 986–996 (2006). [PubMed: 16955546]

2. Hill JW, Hazra TK, Izumi T & Mitra S Stimulation of human 8-oxoguanine-DNA glycosylase by AP-endonuclease: potential coordination of the initial steps in base excision repair. Nucleic Acids Res 29, 430–438 (2001). [PubMed: 11139613]

3. Rodriguez Y & Smerdon MJ The structural location of DNA lesions in nucleosome core particles determines accessibility by base excision repair enzymes. J Biol Chem 288, 13863–13875, doi: 10.1074/jbc.M112.441444 (2013). [PubMed: 23543741]

4. Odell ID, Wallace SS & Pederson DS Rules of engagement for base excision repair in chromatin. J Cell Physiol 228, 258–266, doi:10.1002/jcp.24134 (2013). [PubMed: 22718094]

5. Odell ID, Newick K, Heintz NH, Wallace SS & Pederson DS Non-specific DNA binding interferes with the efficient excision of oxidative lesions from chromatin by the human DNA glycosylase, NEIL1. DNA Repair (Amst 9, 134–143, doi:10.1016/j.dnarep.2009.11.005 (2010). [PubMed: 20005182]

6. Prasad A, Wallace SS & Pederson DS Initiation of base excision repair of oxidative lesions in nucleosomes by the human, bifunctional DNA glycosylase NTH1. Mol Cell Biol 27, 8442–8453, doi:10.1128/MCB.00791-07 (2007). [PubMed: 17923696]

7. Hinz JM Impact of abasic site orientation within nucleosomes on human APE1 endonuclease activity. Mutat Res 766–767, 19–24, doi:10.1016/j.mrfmmm.2014.05.008 (2014).

8. Bilotti K, Tarantino ME & Delaney S Human Oxoguanine Glycosylase 1 Removes Solution Accessible 8-Oxo-7,8-dihydroguanine Lesions from Globally Substituted Nucleosomes Except in the Dyad Region. Biochemistry 57, 1436–1439, doi:10.1021/acs.biochem.7b01125 (2018). [PubMed: 29341606]

9. Bilotti K, Kennedy EE, Li C & Delaney S Human OGG1 activity in nucleosomes is facilitated by transient unwrapping of DNA and is influenced by the local histone environment. DNA Repair (Amst) 59, 1–8, doi:10.1016/j.dnarep.2017.08.010 (2017). [PubMed: 28892740]

10. Maher RL et al. Human cells contain a factor that facilitates the DNA glycosylase-mediated excision of oxidized bases from occluded sites in nucleosomes. DNA Repair (Amst) 57, 91–97, doi:10.1016/j.dnarep.2017.06.029 (2017). [PubMed: 28709015]

11. Czaja W, Mao P & Smerdon MJ The emerging roles of ATP-dependent chromatin remodeling enzymes in nucleotide excision repair. International journal of molecular sciences 13, 11954–11973, doi:10.3390/ijms130911954 (2012). [PubMed: 23109894]

12. Rodriguez Y, Hinz JM & Smerdon MJ Accessing DNA damage in chromatin: Preparing the chromatin landscape for base excision repair. DNA Repair (Amst) 32, 113–119, doi:10.1016/j.dnarep.2015.04.021 (2015). [PubMed: 25957487]

13. Balliano AJ & Hayes JJ Base excision repair in chromatin: Insights from reconstituted systems. DNA Repair (Amst) 36, 77–85, doi:10.1016/j.dnarep.2015.09.009 (2015). [PubMed: 26411876]

14. Peterson CL & Almouzni G Nucleosome dynamics as modular systems that integrate DNA damage and repair. Cold Spring Harbor perspectives in biology 5, doi:10.1101/cshperspect.a012658 (2013).

15. Polo SE & Almouzni G Chromatin dynamics after DNA damage: The legacy of the access-repair-restore model. DNA Repair (Amst) 36, 114–121, doi:10.1016/j.dnarep.2015.09.014 (2015). [PubMed: 26429064]

16. Hinz JM & Czaja W Facilitation of base excision repair by chromatin remodeling. DNA Repair (Amst) 36, 91–97, doi:10.1016/j.dnarep.2015.09.011 (2015). [PubMed: 26422134]

17. Gong F, Kwon Y & Smerdon MJ Nucleotide excision repair in chromatin and the right of entry. DNA Repair (Amst) 4, 884–896, doi:10.1016/j.dnarep.2005.04.007 (2005). [PubMed: 15961354]

18. Waters R, van Eijk P & Reed S Histone modification and chromatin remodeling during NER. DNA Repair (Amst) 36, 105–113, doi:10.1016/j.dnarep.2015.09.013 (2015). [PubMed: 26422133]

19. Sugasawa K UV-DDB: a molecular machine linking DNA repair with ubiquitination. DNA Repair (Amst) 8, 969–972, doi:10.1016/j.dnarep.2009.05.001 (2009). [PubMed: 19493704]

20. Rapic-Otrin V, McLenigan MP, Bisi DC, Gonzalez M & Levine AS Sequential binding of UV DNA damage binding factor and degradation of the p48 subunit as early events after UV irradiation. Nucleic Acids Res 30, 2588–2598 (2002). [PubMed: 12034848]

21. Fischer ES et al. The molecular basis of CRL4DDB2/CSA ubiquitin ligase architecture, targeting, and activation. Cell 147, 1024–1039, doi:10.1016/j.cell.2011.10.035 (2011). [PubMed: 22118460]

22. Kapetanaki MG et al. The DDB1-CUL4ADDB2 ubiquitin ligase is deficient in xeroderma pigmentosum group E and targets histone H2A at UV-damaged DNA sites. Proc Natl Acad Sci U S A 103, 2588–2593, doi:10.1073/pnas.0511160103 (2006). [PubMed: 16473935]

23. Kondo S et al. Assignment of three patients with xeroderma pigmentosum to complementation group E and their characteristics. J Invest Dermatol 90, 152–157 (1988). [PubMed: 3339259]

24. Rapic Otrin V et al. Relationship of the xeroderma pigmentosum group E DNA repair defect to the chromatin and DNA binding proteins UV-DDB and replication protein A. Mol Cell Biol 18, 3182–3190 (1998). [PubMed: 9584159]

25. Dualan R et al. Chromosomal localization and cDNA cloning of the genes (DDB1 and DDB2) for the p127 and p48 subunits of a human damage-specific DNA binding protein. Genomics 29, 62–69, doi:10.1006/geno.1995.1215 (1995). [PubMed: 8530102]

26. Rapic-Otrin V et al. True XP group E patients have a defective UV-damaged DNA binding protein complex and mutations in DDB2 which reveal the functional domains of its p48 product. Human molecular genetics 12, 1507–1522 (2003). [PubMed: 12812979]

27. Oh KS et al. Nucleotide excision repair proteins rapidly accumulate but fail to persist in human XP-E (DDB2 mutant) cells. Photochem Photobiol 87, 729–733, doi:10.1111/j.1751-1097.2011.00909.x (2011). [PubMed: 21388382]

28. Wittschieben BO, Iwai S & Wood RD DDB1-DDB2 (xeroderma pigmentosum group E) protein complex recognizes a cyclobutane pyrimidine dimer, mismatches, apurinic/apyrimidinic sites, and compound lesions in DNA. J Biol Chem 280, 39982–39989, doi:10.1074/jbc.M507854200 (2005). [PubMed: 16223728]

29. Wakasugi M et al. DDB accumulates at DNA damage sites immediately after UV irradiation and directly stimulates nucleotide excision repair. J Biol Chem 277, 1637–1640, doi:10.1074/jbc.C100610200 (2002). [PubMed: 11705987]

30. Reardon JT et al. Comparative analysis of binding of human damaged DNA-binding protein (XPE) and Escherichia coli damage recognition protein (UvrA) to the major ultraviolet photoproducts: T[c,s]T, T[t,s]T, T[6–4]T, and T[Dewar]T. J Biol Chem 268, 21301–21308 (1993). [PubMed: 8407968]

31. Yeh JI et al. Damaged DNA induced UV-damaged DNA-binding protein (UV-DDB) dimerization and its roles in chromatinized DNA repair. Proceedings of the National Academy of Sciences of the United States of America 109, E2737–2746, doi:10.1073/pnas.1110067109 (2012). [PubMed: 22822215]

32. Scrima A et al. Structural basis of UV DNA-damage recognition by the DDB1-DDB2 complex. Cell 135, 1213–1223, doi:10.1016/j.cell.2008.10.045 (2008). [PubMed: 19109893]

33. Ghodke H et al. Single-molecule analysis reveals human UV-damaged DNA-binding protein (UV-DDB) dimerizes on DNA via multiple kinetic intermediates. Proceedings of the National Academy of Sciences of the United States of America 111, E1862–1871, doi:10.1073/pnas.1323856111 (2014). [PubMed: 24760829]

34. D'Errico M et al. New functions of XPC in the protection of human skin cells from oxidative damage. EMBO J 25, 4305–4315, doi:10.1038/sj.emboj.7601277 (2006). [PubMed: 16957781]

35. Parlanti E et al. The cross talk between pathways in the repair of 8-oxo-7,8-dihydroguanine in mouse and human cells. Free Radic Biol Med 53, 2171–2177, doi:10.1016/j.freeradbiomed.2012.08.593 (2012). [PubMed: 23010470]

36. He J et al. A genetically targetable near-infrared photosensitizer. Nat Methods 13, 263–268, doi:10.1038/nmeth.3735 (2016). [PubMed: 26808669]

37. Fouquerel E et al. Targeted and Persistent 8-Oxoguanine Base Damage at Telomeres Promotes Telomere Loss and Crisis. Molecular Cell, doi:10.1016/j.molcel.2019.04.024 (2019).

38. Fujiwara Y et al. Characterization of DNA recognition by the human UV-damaged DNA-binding protein. J Biol Chem 274, 20027–20033 (1999). [PubMed: 10391953]

39. Prasad R, Shock DD, Beard WA & Wilson SH Substrate channeling in mammalian base excision repair pathways: passing the baton. J Biol Chem 285, 40479–40488, doi:10.1074/jbc.M110.155267 (2010). [PubMed: 20952393]

40. Sidorenko VS, Nevinsky GA & Zharkov DO Mechanism of interaction between human 8-oxoguanine-DNA glycosylase and AP endonuclease. DNA Repair (Amst) 6, 317–328, doi:10.1016/j.dnarep.2006.10.022 (2007). [PubMed: 17126083]

41. Mokkapati SK, Wiederhold L, Hazra TK & Mitra S Stimulation of DNA glycosylase activity of OGG1 by NEIL1: functional collaboration between two human DNA glycosylases. Biochemistry 43, 11596–11604, doi:10.1021/bi049097i (2004). [PubMed: 15350146]

42. Prasad R, Dyrkheeva N, Williams J & Wilson SH Mammalian Base Excision Repair: Functional Partnership between PARP-1 and APE1 in AP-Site Repair. PloS one 10, e0124269, doi:10.1371/journal.pone.0124269 (2015). [PubMed: 26020771]

43. Gembka A et al. The checkpoint clamp, Rad9-Rad1-Hus1 complex, preferentially stimulates the activity of apurinic/apyrimidinic endonuclease 1 and DNA polymerase beta in long patch base excision repair. Nucleic Acids Res 35, 2596–2608, doi:10.1093/nar/gkl1139 (2007). [PubMed: 17426133]

44. de Souza-Pinto NC et al. The recombination protein RAD52 cooperates with the excision repair protein OGG1 for the repair of oxidative lesions in mammalian cells. Mol Cell Biol 29, 4441–4454, doi:10.1128/MCB.00265-09 (2009). [PubMed: 19506022]

45. Giuntoli RD et al. DNA-Segment-Facilitated Dissociation of Fis and NHP6A from DNA Detected via Single-Molecule Mechanical Response. Journal of molecular biology 427, 3123–3136, doi:10.1016/j.jmb.2015.07.015 (2015). [PubMed: 26220077]

46. Hadizadeh N, Johnson RC & Marko JF Facilitated Dissociation of a Nucleoid Protein from the Bacterial Chromosome. Journal of bacteriology 198, 1735–1742, doi:10.1128/jb.00225-16 (2016). [PubMed: 27044624]

47. Freudenthal BD, Beard WA, Cuneo MJ, Dyrkheeva NS & Wilson SH Capturing snapshots of APE1 processing DNA damage. Nat Struct Mol Biol 22, 924–931, doi:10.1038/nsmb.3105 (2015). [PubMed: 26458045]

48. Liu L et al. PARP1 changes from three-dimensional DNA damage searching to one-dimensional diffusion after auto-PARylation or in the presence of APE1. Nucleic Acids Res 45, 12834–12847, doi:10.1093/nar/gkx1047 (2017). [PubMed: 29121337]

49. Reardon JT, Bessho T, Kung HC, Bolton PH & Sancar A In vitro repair of oxidative DNA damage by human nucleotide excision repair system: possible explanation for neurodegeneration in xeroderma pigmentosum patients. Proc Natl Acad Sci U S A 94, 9463–9468 (1997). [PubMed: 9256505]

50. Muniandy PA, Thapa D, Thazhathveetil AK, Liu ST & Seidman MM Repair of laser-localized DNA interstrand cross-links in G1 phase mammalian cells. J Biol Chem 284, 27908–27917, doi:10.1074/jbc.M109.029025 (2009). [PubMed: 19684342]

51. Itoh T, Cado D, Kamide R & Linn S DDB2 gene disruption leads to skin tumors and resistance to apoptosis after exposure to ultraviolet light but not a chemical carcinogen. Proc Natl Acad Sci U S A 101, 2052–2057, doi:10.1073/pnas.0306551101 (2004). [PubMed: 14769931]

52. Pines A et al. Differential activity of UV-DDB in mouse keratinocytes and fibroblasts: impact on DNA repair and UV-induced skin cancer. DNA Repair (Amst) 8, 153–161, doi:10.1016/j.dnarep.2008.09.011 (2009). [PubMed: 18996499]

53. Yoon T et al. Tumor-prone phenotype of the DDB2-deficient mice. Oncogene 24, 469–478, doi:10.1038/sj.onc.1208211 (2005). [PubMed: 15558025]

REFERENCES (methods only)

54. Kovtun IV et al. OGG1 initiates age-dependent CAG trinucleotide expansion in somatic cells. Nature 447, 447–452, doi:10.1038/nature05778 (2007). [PubMed: 17450122]

55. Nunez NN, Majumdar C, Lay KT & David SS Fe-S Clusters and MutY Base Excision Repair Glycosylases: Purification, Kinetics, and DNA Affinity Measurements. Methods in enzymology 599, 21–68, doi:10.1016/bs.mie.2017.11.035 (2018). [PubMed: 29746241]

56. Strauss PR, Beard WA, Patterson TA & Wilson SH Substrate binding by human apurinic/apyrimidinic endonuclease indicates a Briggs-Haldane mechanism. J Biol Chem 272, 1302–1307 (1997). [PubMed: 8995436]

57. Beard WA & Wilson SH Purification and domain-mapping of mammalian DNA polymerase beta. Methods in enzymology 262, 98–107 (1995). [PubMed: 8594388]

58. Slupphaug G et al. Properties of a recombinant human uracil-DNA glycosylase from the UNG gene and evidence that UNG encodes the major uracil-DNA glycosylase. Biochemistry 34, 128–138 (1995). [PubMed: 7819187]

59. Chen X et al. Human DNA ligases I, III, and IV-purification and new specific assays for these enzymes. Methods in enzymology 409, 39–52, doi:10.1016/S0076-6879(05)09003-8 (2006). [PubMed: 16793394]

60. Schofield MJ, Lilley DMJ & White MF Dissection of the sequence specificity of the holliday junction endonuclease CCE1. Biochemistry 37, 13042, doi:10.1021/bi985045f (1998).

61. Pollard TD A guide to simple and informative binding assays. Mol Biol Cell 21, 4061–4067, doi:10.1091/mbc.E10-08-0683 (2010). [PubMed: 21115850]

62. Prasad R, Williams JG, Hou EW & Wilson SH Pol beta associated complex and base excision repair factors in mouse fibroblasts. Nucleic Acids Res 40, 11571–11582, doi:10.1093/nar/gks898 (2012). [PubMed: 23042675]

63. Kong M, Beckwitt EC, Springall L, Kad NM & Van Houten B Single-Molecule Methods for Nucleotide Excision Repair: Building a System to Watch Repair in Real Time. Methods Enzymol 592, 213–257, doi:10.1016/bs.mie.2017.03.027 (2017). [PubMed: 28668122]

64. Zhao R et al. DDB2 modulates TGF-beta signal transduction in human ovarian cancer cells by downregulating NEDD4L. Nucleic Acids Res 43, 7838–7849, doi:10.1093/nar/gkv667 (2015). [PubMed: 26130719]
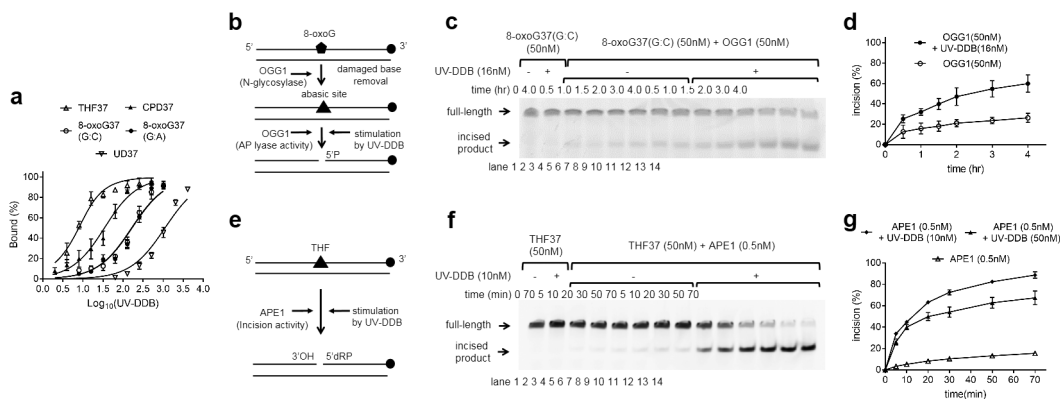
Figure 1. UV-DDB stimulates OGG1 and APE 1 by binding specifically to 8-oxoG:C and abasic sites.

(a). Binding isotherms for THF, CPD, 8-oxoG:C, 8-oxoG:A and undamaged DNA. Data is plotted as mean ± s.e.m. of three independent experiments.

(b). Schematic representation of the DNA substrate containing 8-oxoG and the proposed reaction scheme.

(c). Stimulation of OGG1 incision kinetics by UV-DDB. OGG1 (50nM) was incubated with dsDNA (50nM) containing 8-oxoG:C in the absence (−) or presence (+) of UV-DDB (16nM) at 37°C. Aliquots were withdrawn at each time point and analyzed on a 10% denaturing polyacrylamide gel. Positions of the un-cleaved full-length substrate and incised product are indicated by arrows.

(d). Quantification of the stimulation of OGG1 incision kinetics by UV-DDB in (c). Incision product formation was quantified using GelAnalyzer software. The incision percentage was plotted as mean ± s.d. from seven independent experiments, each run on duplicate gels.

(e). Schematic representation of the DNA substrate containing a THF-site and the proposed reaction scheme.

(f). Stimulation of APE1 incision kinetics by UV-DDB. APE1 (0.5nM) was incubated with the THF37 dsDNA (50nM) in the absence (−) or presence (+) of UV-DDB (10nM) at room temperature. Aliquots were withdrawn at each time point and analyzed on a 10% denaturing polyacrylamide gel. Positions of the un-cleaved full-length substrate and incised product are indicated by arrows.

(g). Quantification of the stimulation of APE1 incision kinetics by UV-DDB in (f). Quantification of the incision product formation was performed using GelAnalyzer software. The incision percentage was plotted as mean ± s.d. from three independent experiments, each run on duplicate gels.
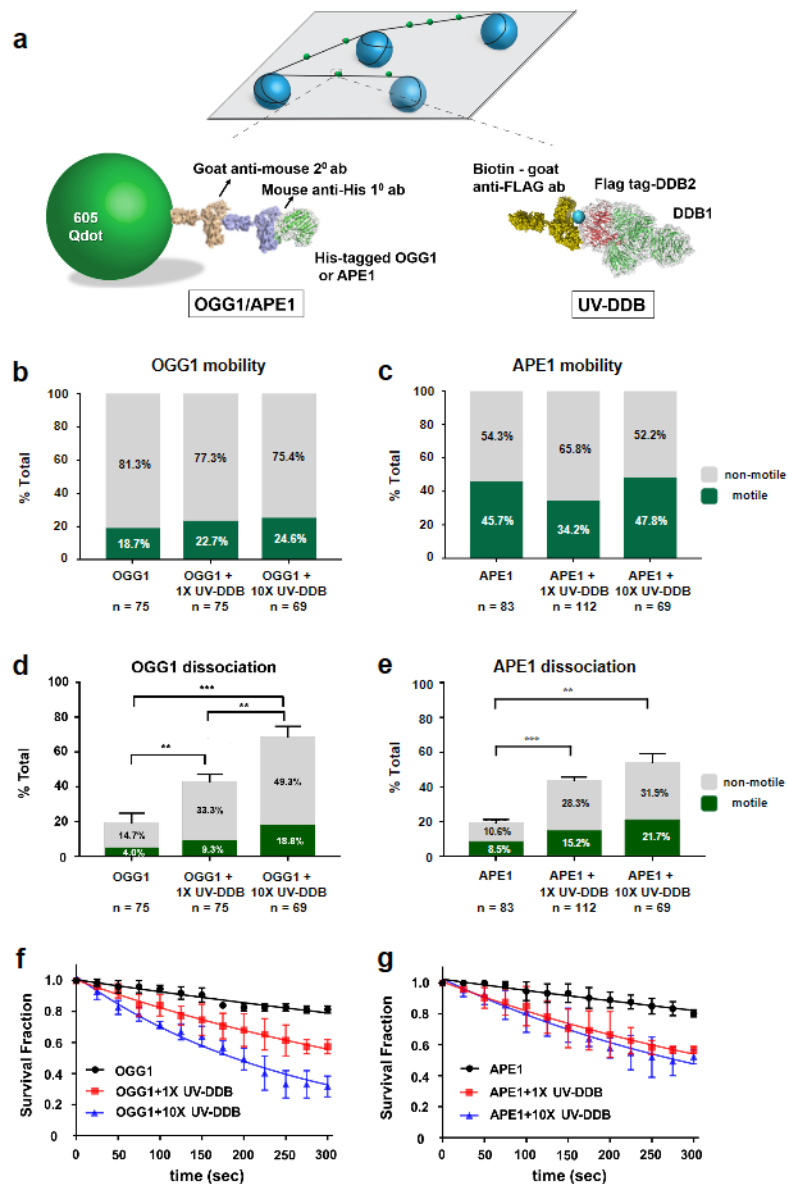
Figure 2. Single molecule analysis reveals UV-DDB stimulates OGG1 and APE1 by facilitated dissociation

(a). Experimental design of DNA tightrope assay to study UV-DDB facilitated dissociation of OGG1 or APE1. (Top) Long DNA substrates with defined abasic sites (THF) every 2 kb are suspended between silica beads. (Bottom, left) His-tagged OGG1 or APE1 are labeled with primary mouse-anti-His antibody and secondary goat-anti-mouse antibody conjugated to a 605 nm Qdot. (Bottom, right) Flag-tagged UV-DDB is bound by primary goat-anti-Flag antibody.

(b). Motility of 605Qdot-labeled OGG1 (green: motile, gray: non-motile) on DNA tightropes containing abasic sites (THF) in the absence or presence of 1X (2.6nM) or 10X (26nM) UV-DDB.

(c). Motility of 605Qdot-labeled APE1 (green: motile, gray: non-motile) on DNA tightropes containing abasic sites (THF) in the absence or presence of 1X or 10X UV-DDB.

(d). Comparison of dissociation percentage of 605Qdot-labeled OGG1 in the absence or presence of unlabeled 1X or 10X UV-DDB. Bar graph data shown as weighted means ± weighted SDs with three independent experiments. (** $p < 0.01$; *** $p < 0.001$ by two-tailed Student's *t* test).

(e). Comparison of dissociation percentage of 605Qdot-labeled APE1 in the absence or presence of unlabeled 1X or 10X UV-DDB. Bar graph data are represented as weighted means ± weighted SDs with three independent experiments. (** $p < 0.01$; *** $p < 0.001$ by two-tailed Student's *t* test).

(f). Effects of UV-DDB on the life times of OGG1-DNA complexes. Data plotted as the mean ± SEM from three independent experiments. For each condition, survival fraction decay is fit to a single exponential decay function to obtain the half-life.

(g). Effects of UV-DDB on the life times of APE1-DNA complexes. Data plotted as the mean ± SEM from three independent experiments. For each condition (without UV-DDB or with 1X/10X UV-DDB), survival fraction decay is fit to a single exponential decay function to obtain the half-life.
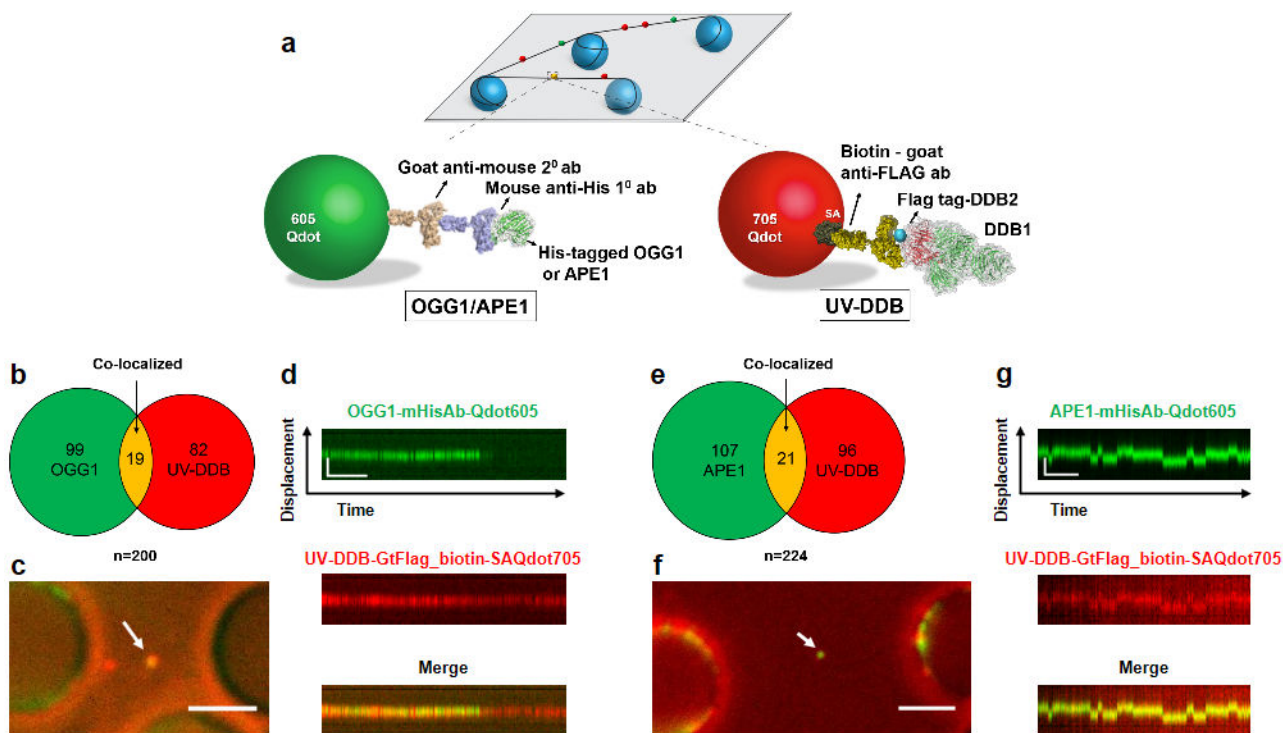
Figure 3. Single molecule co-localization of UV-DDB with OGG1 or APE1 on abasic DNA tightropes.

(a). Schematic of the DNA tightrope assay. Long DNA substrates with abasic sites every 2 kb were suspended between 5μm poly-L-lysine coated silica beads. Anti-His primary antibody was used to link the His-tagged OGG1 or APE1 to the 605Qdot. Biotin conjugated anti-Flag primary antibody was used to link Flag-tagged UV-DDB to streptavidin-coated 705Qdot. Uniquely labeled OGG1/APE1 and UV-DDB were observed interacting on abasic DNA tightropes in real time and their behavior and frequency of co-localization was recorded.

(b). Venn diagram showing number of proteins that co-localized (yellow) on abasic (THF) tightropes or were observed separately for 605Qdot-labeled OGG1 (green) with 705Qdot-labeled UV-DDB (red) in the dual-color assay.

(c). Image of co-localized (yellow) Qdot-labeled OGG1 (green) and UV-DDB (red) on abasic (THF) tightrope suspended between beads. Scale bar represents 2.5μm. Arrow points to co-localized particle.

(d). Kymograph of co-localized OGG1 and UV-DDB. Top, OGG1 (green); middle, UV-DDB (red); bottom, merged (yellow). Horizontal and vertical scale bars represent 50s and 2kb, respectively.

(e). Venn diagram showing number of proteins that co-localized (yellow) on abasic (THF) tightropes or were observed separately for 605Qdot-labeled APE1 (green) with 705Qdot-labeled UV-DDB (red) in the dual-color assay.

(f). Image of co-localized (yellow) Qdot-labeled APE1 (green) and UV-DDB (red) on abasic (THF) tightrope suspended between beads. Scale bar represents 2.5μm. Arrow points to co-localized particle.

(g). Kymograph of co-localized APE1 and UV-DDB. Top, APE1 (green); middle, UV-DDB (red); bottom, merged (yellow). Horizontal and vertical scale bars represent 50s and 2kb, respectively.

See also Figure S4 and Videos S1 and S2.
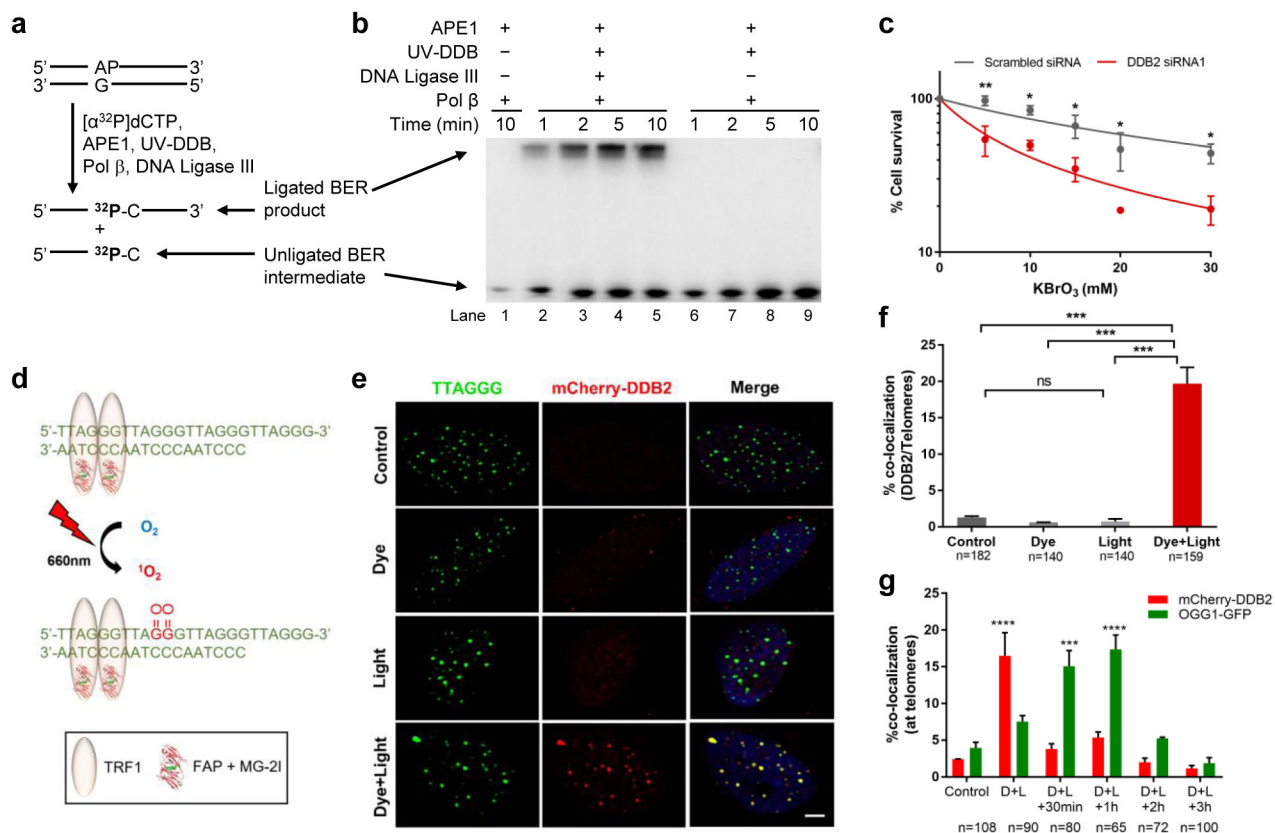
Figure 4. UV-DDB stimulates BER

(a). Schematic representation of the in vitro BER substrate and the expected BER products after gap-filling (insertion of $[\alpha^{32}P]$-dCTP) and ligation steps.

(b). BER time course and the influence of UV-DDB on the activity of BER components. UDG pretreated DNA (200 nM) was incubated with APE1 (1 nM) in the absence (–) or presence (+) of UV-DDB (50 nM), Pol β (20 nM) and DNA ligase III (250 nM). The migration positions of the ligated BER product and unligated BER intermediate are indicated. The results shown are representative of three independent experiments. Quantitation of lane 1 versus lane 9, from three independent experiments shows a 30-fold difference in $[\alpha^{32}P]$-dCTP incorporation stimulated by UV-DDB.

(c). Cell survival curves of BJ-hTERT cells transfected with scrambled or DDB2 siRNA and treated with a range of concentration of $KBrO_3$. Data represent mean ± SEM from three independent experiments, each performed in triplicate. (* $p<0.05$; ** $p<0.01$ by two-tailed Student's *t* test)

(d). Schematic description of the TRF1 FAP system. U2OS cells stably expressing the TRF1 FAP were treated with 100nM dye (MG2I) and light (660nm) for 10 minutes to generate singlet oxygen at the telomeres leading to the formation of 8-oxoG.

(e). Immunofluorescence images depicting the recruitment of mCherry-DDB2 to telomeres after specifically inducing 8-oxoG at the telomeric region. Scale bar: 5μm

(f). Bar graph showing quantification of (e), where horizontal bars indicate mean ± SEM from two independent experiments (*** $p<0.001$ by one-way ANOVA).
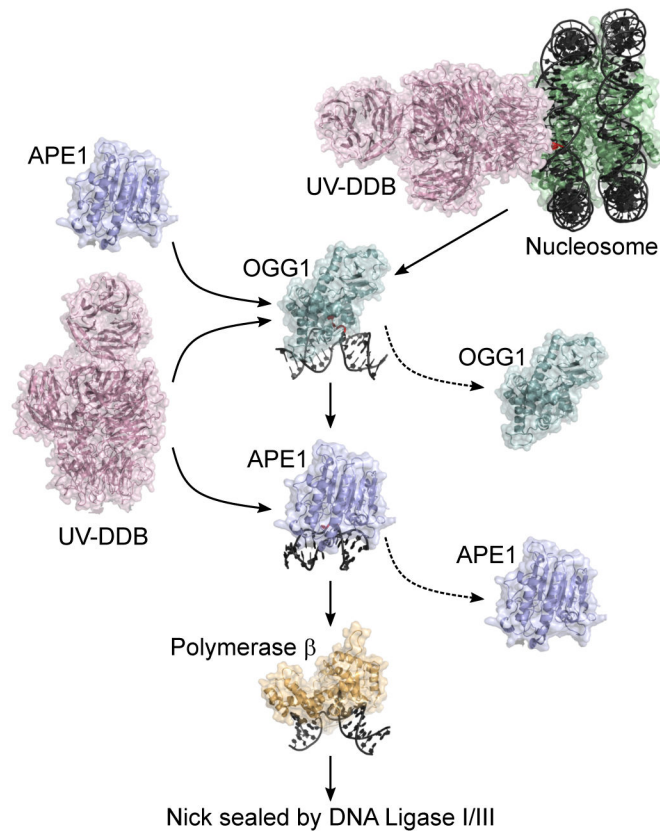
(g). Bar graph quantifying the DDB2 and OGG1 foci at telomeres over a 3-hour time course. Data represents mean ± SEM from two independent immunofluorescence experiments. (*p<0.05; ** p<0.01 by two-way ANOVA).

Figure 5.
Schematic representation of the proposed BER pathway including UV-DDB is illustrated. UV-DDB appears to be rapidly recruited to damaged sites in chromatin and help facilitate processing by OGG1, MUTYH (not shown) and APE1. Biochemical and single molecule data suggest that UV-DDB transiently associates with OGG1 or APE1 at abasic sites to increase their turnover and stimulated BER (see text for description).

Table 1.

Apparent equilibrium dissociation constant (K_d) of UV-DDB to different kinds of DNA lesions, related to Figure 1

Substrate (dsDNA)	K_d (nM)[a]
THF37	3.9 ± 0.5
CPD37	30.4 ± 2.4
8-oxoG37(G:C)	159.6 ± 12.4
8-oxoG37(G:A)	163.8 ± 14.8
UD37	1108.0 ± 95.5

[a] Apparent equilibrium dissociation constant (K_d) were determined from data presented in Figure 1a. These data are based on three independent experiments. The K_d value is the best-fit value to the three points $\pm$ the s.e. of the fit to the observed data.